Effects of nanoparticle heating on the structure of a concentrated aqueous salt solution

Effects of nanoparticle heating on the structure of a concentrated aqueous salt solution

Julien O. Sindt,[1] Andrew J. Alexander,[2] and Philip J. Camp[2, 3, a)]

[1)] *School of Engineering, University of Edinburgh, Mayfield Road, Edinburgh EH9 3JL, Scotland*

[2)] *School of Chemistry, University of Edinburgh, David Brewster Road, Edinburgh EH9 3FJ, Scotland*

[3)] *Department of Theoretical and Mathematical Physics, Institute of Natural Sciences and Mathematics, Ural Federal University, 51 Lenin Avenue, Ekaterinburg, 620000, Russia*

(Dated: 14 November 2017)

The effects of a rapidly heated nanoparticle on the structure of a concentrated aqueous salt solution are studied using molecular dynamics simulations. A diamond-like nanoparticle of radius 20 Å is immersed in a sodium-chloride solution at 20% above the experimental saturation concentration and equilibrated at $T = 293$ K and $P = 1$ atm. The nanoparticle is then rapidly heated to several thousand degrees Kelvin, and the system is held under isobaric-isoenthalpic conditions. It is observed that after 2–3 ns, the salt ions are depleted far more than water molecules from a proximal zone 15–20 Å from the nanoparticle surface. This leads to a transient reduction in molality in the proximal zone, and an increase in ion clustering in the distal zone. At longer times, ions begin to diffuse back into the proximal zone. It is speculated that the formation of proximal and distal zones, and the increase in ion clustering, plays a role in the mechanism of nonphotochemical laser-induced nucleation.

[a)] Corresponding author: philip.camp@ed.ac.uk

I. INTRODUCTION

Nonphotochemical laser-induced nucleation (NPLIN) is the phenomenon whereby nanosecond laser pulses of near-infrared or visible light incident upon supersaturated solutions or melts cause nucleation and growth of solid solute.[1–3] Because the solutions are transparent at the laser wavelengths used, the mechanism is thought to be nonphotochemical. This is to be contrasted with nucleation caused by ionization of molecules or radical formation through the absorption of short laser pulses at higher intensities and shorter wavelengths.[4–7] Several distinct NPLIN mechanisms have been proposed. The first mechanism involves the optical Kerr effect (OKE), whereby the electric field of the light interacts with the anisotropy of solute molecules in clusters, causing molecules to align and the clusters to become viable as crystal nuclei. This mechanism also offers an explanation for the putative effect of polymorph selection by linearly polarized and circularly polarized light.[1–3] It should be noted, though, that simulations suggest that the field strengths employed in experiments are too low to cause sufficient orientational bias.[8] Moreover, recent experiments have shown that the effects of light polarization in NPLIN are much weaker than the original experiments suggested.[9,10] The second mechanism was inspired by NPLIN having being demonstrated in simple ionic solutions,[11–17] in which the OKE is unlikely to occur at the atomic scale. This mechanism revolves around the dielectric polarization and reduction in free energy of existing solid-like solute clusters which have sub-critical radii in the absence of a field, but super-critical radii when the electric field of the laser is switched on.[11] In this scenario, a small fraction of existing solid-like solute clusters become viable crystal nuclei during the laser pulse, and go on to grow. The attractive features of this model are that almost all experimentally observed trends can be rationalized quantitatively in terms of physical and molecular parameters such as temperature, supersaturation, laser wavelength, solute and solvent refractive index, etc.[11–14] A similar model has been proposed for the nucleation of metallic nanoparticles.[18,19]

There are, however, some key experimental observations that cannot be captured by these models: NPLIN is only observed when the laser pulse is above a threshold intensity (depending on material) and above a threshold duration (somewhere around 5–100 ps). For instance, in the dielectric polarization model, NPLIN should be observed at all laser intensities, and there is no explicit account taken of the pulse duration. Moreover, none of the

mechanisms take account of impurity particles. It has been observed that careful filtration (which can never remove all small impurity particles) reduces significantly the propensity for NPLIN, but it does not stop the effect, and it can be recovered by the addition of iron-oxide nanoparticles.[9,17,20] The important feature of impurity particles is that they could absorb the laser light, causing rapid heating of the particle, localized heating of the solution, and any number of concomitant effects such as localized vaporization, bubble formation and collapse, shock waves, etc. that could initiate nucleation of the solute. Such processes are well known from experiments and simulations.[21–29]

This work reports simulations of a rapidly heated spherical nanoparticle (NP) in a supersaturated aqueous sodium-chloride solution, and the effects on the solution structure as the thermal energy of the particle diffuses into the solution under conditions of constant pressure. The salt concentration is chosen so that it is as high as possible without seeing homogeneous nucleation in a pure solution on the simulation time scale. It is found that at equilibrium, prior to NP heating, the distribution of hydrated ions is uniform, except for a molecular layer of pure water near to the particle surface. Over the course of 2–3 ns following the instantaneous heating of the NP, the solution expands as the temperature increases, but factoring out this expansion, the ion concentration near the NP drops far more than the water concentration. This depletion of ions near the NP causes an excess of ions away from the NP, and an increase in ion clustering, both of which could give rise to nucleation in the distal zone. In this scenario, the heat gained by the solution near the NP would have to diffuse into the bulk, and it is not clear how to simulate this process without moving to much larger systems (the current simulations involve around 2×10^5 atoms) or without introducing an artificial thermal sink. Therefore, homogeneous nucleation of the salt has not been observed in the simulations, but this work provides some foundation for future studies.

The rest of this article is arranged as follows. The simulation model and protocol are described in Section II. The results are presented in Section III:[30] firstly, simulations of supersaturated pure solutions were used to determine the highest concentration of ions at which spontaneous homogeneous nucleation will not be observed on the simulation time scale; secondly, a spherical NP was introduced to the solution, the system was equilibrated, and then rapid heating of the NP was carried out. The results are discussed and conclusions are presented in Section IV.

II. MODEL AND METHODS

A. Pure solutions

Atomistic molecular dynamics (MD) simulations were carried out on pure aqueous sodium chloride solutions in the isothermal-isobaric (NPT) ensemble at temperature $T = 293$ K and pressure $P = 1$ atm using a Nosé-Hoover thermostat/barostat. 500 ion pairs were simulated at various concentrations, as given in Table I. The concentrations are also shown relative to the experimental saturation concentration (molality) of $b_{\rm sat} = 6.147$ mol kg^{-1} at $T = 293$ K.[31] All interactions were described using a combination of Lennard-Jones and Coulomb interactions. The TIP3P water model optimized for Ewald summations was used.[32,33] This and several other popular models have been assessed in comparison to structural and thermodynamic data from experiments on supercritical water up to temperatures of 800 K, and of course at high pressures.[34–36] The key point is that the agreement between simulation and experiment is generally good, and so such water models are adequate for the current study which is focused on the qualitative effects of NP heating. Na^+ and Cl^- ions were described using parameter sets developed by Dang and coworkers.[37,38] The LJ range and energy parameters σ and ε, respectively, and the particle charges q, are listed in Table II. With this combination of forcefields the solubility of NaCl has previously been estimated to be 4.84 kg mol^{-1}.[39] LJ interactions were truncated at 12 Å and the long-range Coulomb interactions were handled using the particle-particle particle-mesh method. The equations of motion were integrated with the Tuckerman-Verlet algorithm with a time step of 1 fs for a total of 25 ns for each concentration considered. All simulations were carried out using LAMMPS.[40,41]

B. Solutions with a heated nanoparticle

The compositions of simulations involving a NP are given in Table I. A solid NP was formed from diamond-like carbon (bond length 1.54 Å and bond angle 109.5°) by cutting all bonds beyond a radius 20 Å from a central atom, and then removing any atoms with fewer than three bonds intact. The solid NP is shown in Fig. 1(a). Although the chemical details are irrelevant here, the LJ parameters of the NP atoms were set at typical values for neutral sp^3-hybridized carbon atoms.[42,43] The bond lengths and bond angles

were constrained by harmonic potentials with spring constants $k_r = 496.0$ kcal mol^{-1} Å^{-2} and $k_\theta = 63.0$ kcal mol^{-1} deg^{-2}, respectively, which are typical values for hydrocarbons. First, NaCl(aq) containing a NP was simulated as above for 1 ns in the NPT ensemble at $T = 293$ K and pressure $P = 1$ atm. Then, instantaneous heating of the NP was carried out by reassigning the NP atom velocities drawn from the Maxwell-Boltzmann distribution at either 5293 K or 10293 K, maintaining the NP at that temperature in the NVT ensemble for 10 ps, and then continuing the dynamics in the isoenthalpic-isobaric (NPH) ensemble.

Some comments on the choice of temperature and ensemble are in order. Basically, the choice of heating temperature was made in order to see an effect, but previous work on laser-heated colloidal particles shows that temperatures of several thousand degrees Kelvin are to be expected with pulse wavelengths, intensities, and durations similar to those used in NPLIN experiments.[44] In a typical NPLIN experiment, a NP with radius $R = 2$ nm subjected to a laser pulse with peak power $I = 25$ MW cm^{-2} over a time period $\Delta t = 100$ ps could absorb up to $E = \pi R^2 I \Delta t = 3 \times 10^{-16}$ J. Assuming total absorption and a constant heat capacity of $C_P = 6$ J K^{-1} mol^{-1}, the temperature rise of 5851 atoms would be over $E/C_P = 5000$ K, which of course is immense, and would at least cause melting of the NP. As shown in Ref. 28 the behavior of the surrounding solution depends mainly on the total amount of energy pumped in, as long as that heating happens quickly, meaning 10–100 ps as in the current work. So, the NP temperatures of 5293 K or 10293 K are chosen merely to inject enough thermal energy in to the system to raise the solution temperature sufficiently high; the most important thing is the temperature of the solution. To check that the total energy, rather than the peak NP temperature, is most important, simulations were also carried out with a hollow NP heated to $T = 10293$ K. The hollow NP is shown in Fig. 1(b). As shown in Table I, the hollow NP contains 3378 atoms, and so the total energy pumped in to the system is about 58% of that of the solid NP at the same temperature. In all cases, the maximum temperature of the solution reached in the simulations is about 550 K, which is typical of the temperatures reached in experiments,[22–25] and is in the temperature ranges where classical water models have been tested against experimental data.[34–36]

The reason for switching ensemble from NPT to NPH after heating is that a constant-volume ensemble would inhibit thermal expansion of the solution around the NP, and a constant-temperature ensemble would require an artificial protocol for dissipating excess thermal energy from some part of the system. A natural means of thermostatting the system

would be to consider a larger system, and designate some part of it as a thermal sink, but the simulations already involved around 2×10^5 atoms. These simulations have therefore captured the effects of the heated NP on the nearby solution, but not the subsequent cooling process and any resulting crystal nucleation and growth.

III. RESULTS

A. Pure solutions

The first step was to determine a suitable salt concentration that it is as high as possible, but without causing homogeneous nucleation on the simulation time scale.[45,46] To this end, the salt solutions listed in Table I were studied. Crystal nuclei were identified using two separate criteria. In the first criterion, an ion was considered in a crystalline state if it had five or more neighbors within a distance r_n.[47,48] The cut-off distance was chosen to be the position of the first local minimum in the Na^+–Cl^- radial distribution function, $r_\mathrm{n} = 3.80$ Å. This is in excellent agreement with existing simulation work on concentrated brines, albeit with the SPC/E water model, which also showed that the position of the minimum is essentially constant at concentrations up to 8 mol kg^{-1}.[35] Figure 2(a) shows the probability of an ion having N_n neighbors, from simulations at $b = b_\mathrm{sat}$ and $b = 1.5b_\mathrm{sat}$. Choosing a small number of neighbors would not distinguish strongly between low and high supersaturation. The threshold of five or more neighbors was chosen as a compromise between sensitivity and statistical significance.

The second criterion was based on the local bond-order parameter $Q_4 \geq 0.45$ with the same distance-based cutoff, r_n.[49–56] With these definitions, the ions satisfying the local bond-order criterion were a subset of those satisfying the simple distance-based criterion. Ions on the surface of a cluster may not satisfy a crystalline-cluster criterion, but they were included in the definition of a cluster through being directly bonded to a crystalline ion.

Figures 1(c) and (d) show snapshots of the ions satisfying the distance-based criterion in simulations with $b = b_\mathrm{sat}$ and $b = 1.5b_\mathrm{sat}$. Figures 1(e), (f), and (g) show snapshots of all ions, ions satisfying the distance-based criterion, and ions satisfying the local bond-order criterion, respectively, in a simulation with $b = 1.4b_\mathrm{sat}$. These images show that crystalline clusters were present in the system at high concentrations, and that the distance-based and

local bond-order criteria gave qualitatively similar results.

The lifetime of crystalline clusters was studied using the time correlation function

$$C_\Theta(t) = \frac{\langle \Theta(t)\Theta(0)\rangle}{\langle \Theta(0)\Theta(0)\rangle} \tag{1}$$

averaged over all ions. $\Theta(t) = 1$ if an ion was crystalline for all times from 0 to t, and $\Theta(t) = 0$ otherwise. Since $\Theta^2 = \Theta$, $\langle \Theta(0)\Theta(0)\rangle = \langle \Theta(0)\rangle$ represents the average fraction of ions that are considered crystalline (f_c). $C_\Theta(t)$ from the distance-based criterion is shown in Fig. 2(b), and there is clear change in behavior between $1.2b_\mathrm{sat}$ and $1.3b_\mathrm{sat}$, with the correlation function decaying much more rapidly at the lower concentrations. The tails of the correlation functions are not reliable, since at long times the numbers of remaining ions with $\Theta = 1$ are very small. Figure 2(c) shows $f_\mathrm{c} = \langle \Theta(0)\Theta(0)\rangle$ from both the distance-based and local bond-order criteria. Although the proportion of crystalline particles depends on the criterion used, it grows roughly linearly with increasing concentration. The residence time for an ion in a crystalline state is estimated using the relation

$$t_\mathrm{res} = \int_0^\infty C_\Theta(t)\ \mathrm{d}t. \tag{2}$$

The integral is carried out up to 25 ns, but given the artificially rapid decay of $C_\Theta(t)$ at long times, this is an underestimate of the true residence time, particularly at high concentration. Figure 2(d) shows t_res from both the distance-based and local bond-order criteria. There is a sharp increase in the residence time between $1.2b_\mathrm{sat}$ and $1.3b_\mathrm{sat}$, irrespective of the crystallinity criterion used. With $b \leq 1.2b_\mathrm{sat}$ the lifetime is less than one nanosecond. On the basis of these results, simulations with a NP were carried out with a salt concentration $b = 1.2b_\mathrm{sat}$, so that there is the maximum number ions to improve statistics on local temperature, density, molality, etc., but with no long-lived crystalline clusters present in the system.

B. Solutions with a solid nanoparticle at $T = 5293$ K

Figure 3 shows radial profiles of the kinetic temperatures of the NP, water, and ions, averaged over spherical shells, and averaged over 0.1 ns intervals at various times before and after heating the NP to $T_\mathrm{NP}(0) = 5293$ K. Firstly, the temperature within the NP [Fig. 3(a)] is roughly uniform except for the very center where there are few atoms and the statistics are poor. The temperatures of the water and ions [Figs. 3(b)–(d)] are equal at all positions

and times, except for at the very surface of the NP, where the numbers of molecules and ions contributing to the apparent temperatures are low. There is a considerable temperature gradient until around 1 ns, after which the temperature is uniform. After 2.8 ns the solution temperature is approximately 420 K, the NP temperature is still about 630 K, and the solution profiles are changing very slowly, and so this is the end of the run. This is still in a nonequilibrium state, however, because of the temperature difference between the NP and the solution.

The structure of the solution near the NP is detailed next. Figure 4(a) shows the radial mass-density profile of water. At equilibrium, before heating, there is a strong peak at around 3 Å from the NP surface. On heating, this primary peak decreases, and the overall density decreases due to box expansion from 129 Å to 134 Å. To factor out the trivial change in mass density due to expansion, Fig. 4(b) shows the results scaled by the quantity

$$f(t) = \frac{\bar{V}(t) - V_{\mathrm{NP}}}{\bar{V}(0) - V_{\mathrm{NP}}} \tag{3}$$

where $\bar{V}(t)$ is the average box volume over the 0.1 ns interval, and $V_{\mathrm{NP}} = 33510$ Å^3 is the nominal volume of the NP. The scaled data show more clearly the loss of water structure near the NP.

The orientations of the water molecules near the NP surface were examined by calculating the two order parameters

$$P_1 = \langle(\hat{\boldsymbol{\mu}} \cdot \hat{\boldsymbol{r}})\rangle \tag{4}$$

$$P_2 = \frac{1}{2}\left\langle 3(\hat{\boldsymbol{\mu}} \cdot \hat{\boldsymbol{r}})^2 - 1\right\rangle \tag{5}$$

where $\hat{\boldsymbol{\mu}}$ is the unit vector aligned with the dipole moment of a water molecule, and $\hat{\boldsymbol{r}}$ is the unit vector pointing from the center of the NP to the oxygen atom. A random distribution of $\hat{\boldsymbol{\mu}}$ gives $P_1 = 0$ and $P_2 = 0$, while if $\hat{\boldsymbol{\mu}}$ is oriented parallel (perpendicular) to $\hat{\boldsymbol{r}}$ then $P_1 = \pm 1$ and $P_2 = 1$ ($P_1 = 0$ and $P_2 = -\frac{1}{2}$). Only those particles in the immediate vicinity of the NP and where the local density is maximal ($22.50 \leq r \leq 22.75$ Å) were included in the average as both order parameters decay rapidly to zero beyond this region. The results are shown in Figs. 5(a) and (b). At equilibrium P_1 is small and positive, meaning that the negative (oxygen) end of the dipole is closer to the NP; this is presumably to achieve both favorable oxygen-NP van der Waals interactions and H-bonding interactions within the surrounding water layer. Following the heat pulse in to the NP, the small degree of

polarization in the radial direction drops rapidly and then decreases slowly. At equilibrium, P_2 is significantly less than zero, meaning that the dipole moments are aligned preferentially in a tangential plane with respect to the NP surface. On heating, the degree of ordering drops sharply and then slowly decreases, but does not disappear altogether. Note that bulk water undergoes polarization in a uniform thermal gradient,[57–63] but a macroscopic polarization is not observed here due to the transient thermal gradient and the small numbers of molecules under examination.

Figure 6 shows the density profiles for the ions, in both unscaled and scaled versions. At equilibrium and after heating there is a significant depletion of ions from the zone within about 5 Å of the NP surface, which is a well-known effect from simulations of nonpolarizable ions at solid-solution and air-solution interfaces.[64–67] This is because it is more energetically favorable for the small, nonpolarizable ions to have full hydration shells. Large, polarizable ions are surface active because of the extra polarization arising from asymmetric solvation at interfaces. After heating, there is even more depletion of ions near the NP surface, and this is apparent in both the unscaled and scaled density profiles. Roughly speaking, the ion density decreases most significantly within about 15 Å from the NP surface. The density profiles after 2.2 ns and 2.8 ns are similar, but at the end it appears that ions are starting to diffuse back into the proximal zone.

The molality profiles of the ions are shown in Figs. 7(a) and (b). There is no need for scaling here because the molality is proportional to the ratio of numbers of ions and water molecules, and this remains unchanged under isotropic expansion of the whole system. On heating, the molalities of both ions decrease within about 15 Å from the NP surface over the first 2.2 ns. At the end of the simulation, it looks like ions are starting to diffuse back into the proximal zone. The molality profiles are too noisy to identify systematically a boundary between proximal and distal zones. In an effort to remove this noise, molalities for each ion type have been calculated within a radius r [$b_<(r)$] and beyond a radius r [$b_>(r)$], and averaged over 0.1 ns intervals. Although the individual functions are still quite noisy, the ratio

$$\beta(r) = \frac{b_<(r)}{b_>(r)} \tag{6}$$

is smooth and practically the same for each ion type, as shown in Fig. 5(c). At each time, $\beta(r) < 1$ shows that the molality within a radius r is lower than that beyond r. Turning back to Fig. 7(a) and (b), the proximal zone after 2.2 ns is $r \lesssim 35$ Å, and at this radius

$\beta(r) \simeq 0.66$. This suggests a simple criterion $\beta(r^*) = 2/3$ for identifying the boundary between the proximal and distal zones.[68] Figure 5(d) shows the boundary position r^* as a function of time. At equilibrium, r^* is within a few molecular layers of the NP surface, but during 2.2 ns after heating, it increases to a maximum value of about 35 Å, before starting to decrease. After 2.2 ns, the average molality in the distal zone ($r \geq r^*$) is 2–3% larger than the overall molality in the system, and this deviation is small compared to the natural fluctuations in the local molality.

Figures 5(e) and (f) show the fractions of ions considered to be in crystalline environments according to the distance-based and bond-order criteria described in Section III A. According to the distanced-based criterion [Fig. 5(e)] the fraction of clustered ions increases with time and peaks at $t = 2.2$ ns, the same time as the proximal zone is largest. This can be understood as a consequence of the loss of hydration through heating and expansion, and the subsequent clustering of ions. The results using the bond-order criterion [Fig. 5(f)] show the same behavior, but the values are much lower as they capture a subset of the ions identified through the distance-based criterion.

C. Solutions with a solid nanoparticle at $T = 10293$ K

The results from the previous section suggest that, upon NP heating, ions are pushed away from the NP surface far more than the water molecules. This effect is more pronounced when the NP is heated to a higher temperature of $T_{\mathrm{NP}}(0) = 10293$ K. Figure 8 shows the radial temperature profiles for the NP, water, and ions. As before, the temperature profiles in the solution become uniform after about 1 ns, and the temperature only slowly increases after that. It was thought that the increased temperature might lead to spontaneous vaporization (or explosive boiling) of the water, which from experiments occurs in the region of $0.8T_{\mathrm{c}} = 520$ K[69,70] (for TIP3P water this would be about 462 K[71]). In Lennard-Jones fluids, nanobubbles are formed spontaneously at about $0.9T_{\mathrm{c}}$.[28] The unscaled and scaled water-density profiles are shown in Figs 4(c) and (d), respectively; over 2.8 ns the box length increases from 129 Å to 145 Å. As before, the water structuring near the NP surface is reduced with increasing temperature, but there is no sign of spontaneous vaporization near the NP surface, despite the temperature reaching about 550 K after 2.8 ns. The orientational order parameters in Figs. 5(a) and (b) show the same trends as those for the solid NP

at lower initial temperature, except that there is a greater loss of ordering associated with the higher temperatures.

The density profiles of the ions are shown in Fig. 9 and there is an enormous depletion of ions from the region within 20–25 Å of the NP surface. The molality profiles in Figs. 7(c) and (d) show the same thing, emphasizing the formation of a proximal region where ions are depleted. The boundary r^* between proximal and distal zones was estimated using the criterion described in Section III B, and the results are shown in Fig. 5(d). The boundary reaches $r^* \simeq 45$ Å after 2.2 ns, and moves back towards the NP thereafter. After 2.2 ns, the average molality in the distal zone ($r \geq r^*$) is 4–5% higher than the overall molality. System configurations are shown in Figs. 10(a)–(d) (Multimedia view): snapshots are shown at equilibrium, and 0.4, 1.6, and 2.8 ns after NP heating; a movie is available online. Figures 10(c) and (d) clearly show the proximal zones where the ion concentration is low, and the distal zones where the ion concentration is high and there is a high degree of clustering.[72] Figure 10(d) shows that some clustered ions have diffused back towards the NP after 2.8 ns.

The fractions of clustered ions identified through the distance-based and bond-order criteria are shown in Figs. 5(e) and (f), respectively. In both cases, f_c increases with time, again reflecting the loss of hydration and expansion of the system on heating. Figures 10(e)–(h) show the clustered ions at equilibrium and 2.8 ns after heating, for both the distance-based criterion [(e) and (f)] and the bond-order criterion [(g) and (h)]. Clearly there are a lot more small clusters after heating, but nothing that yet resembles a crystal nucleus.

D. Solutions with a hollow nanoparticle at $T = 10293$ K

Finally, a simulation was carried out with a hollow NP heated to $T_{\rm NP}(0) = 10293$ K, to see what effect the total heat content has on the solution structure. Figure 11 shows the radial temperature profiles for the NP, water, and ions. The radius of the hollow NP is slightly higher than that of the solid NP due to the missing cohesive interactions with core atoms. The hollow NP cools faster than the solid particle in all cases; within 0.1 ns the hollow NP is at around 8500 K, the solid NP with $T_{\rm NP}(0) = 5293$ K is at around 5000 K, and the solid NP with $T_{\rm NP}(0) = 10293$ K is at around 9500 K. The key comparison is between the hollow NP with $T_{\rm NP}(0) = 10293$ K and the solid NP with $T_{\rm NP}(0) = 5293$ K, since the heat contents are similar. After 2.8 ns the hollow NP is at 435 K while the solid NP is

at 630 K. In the solution with the hollow NP as compared to the solid NP, the transient temperature gradient is higher, a uniform temperature is achieved faster, and the solution temperature after 2.8 ns is slightly higher (450 K as compared to 425 K) possibly reflecting the 12% higher initial heat content. Figures 12(a) and (b) show the unscaled and scaled versions of the water density. The equilibrium water density near the hollow-NP surface is similar to that near the solid-NP surface, but it decreases to about 1400 kg m^{-3} after 2.8 ns, while with the solid NP the density is about 1200 kg m^{-3} [Fig. 4(a)]. The orientational order parameters are shown in Figs. 5(a) and (b). The initial behavior of P_1 is similar to that for the solid NP with $T_{\rm NP}(0) = 10293$ K, reflecting the rapid initial heating of water near the NP surface. At longer times, the degree of ordering approaches that seen with the NP at $T_{\rm NP}(0) = 5293$ K. Note that the values in the range $0 \leq P_1 \leq 0.06$ correspond to a change in the average angle of only 4°, so the effects are small. P_2 shows that there is less disruption to the orientational ordering in the case of the hollow NP as compared to the solid NPs.

The solution molalities [Figs. 12(c) and (d)] do not show as much ion depletion as in the cases with solid NPs, and this is also apparent from the ion densities shown in Fig. 13. The values of r^* shown in Fig. 5(d) suggest that the proximal zone does not extend very far in to the solution, reaching $r^* \simeq 32$ Å after 1.0 ns, and decreasing thereafter. After 1.0 ns, the average molality in the distal zone ($r \geq r^*$) is 1–2% higher than the overall molality.

The fraction of clustered ions is presented in Figs. 5(e) and (f). According to both the distance-based and bond-order criteria, the increase in clustering is less than with the solid NPs, which is consistent with the smaller proximal zone and the less-pronounced accumulation of ions in to the distal zone.

Overall, heating the hollow NP still leads to a transient depletion of ions nearby, but the proximal zone is smaller and shorter lived than with the solid NPs. This could be due to the higher proportion of surface atoms and the more rapid cooling of the hollow NP. With solid NPs, the main depletion of ions occurs after about 0.4 ns, when there is still a significant temperature gradient in the solution. With the hollow NP, the temperature gradient in the solution is much less after 0.4 ns.

IV. DISCUSSION

As outlined in the Introduction, recent experimental evidence points to a mechanism for NPLIN that involves heating of impurity NPs by pulsed laser light.[17,20] In the present work, computer simulations have been used to explore the effect of a heated NP on the structure of a moderately supersaturated solution of sodium chloride. The solution concentration was made as high as possible without homogeneous nucleation being observed on the simulation timescale, which is a minimum requirement to match up with experimental procedures. Crystalline clusters were detected using both distance-based and bond-order criteria, and the lifetimes of clusters were examined using an appropriate time autocorrelation function.

The presence of a heated NP was found to have dramatic effects on the solution structure. Firstly, a transient temperature gradient is set up in the solution, which leads to a rapid reduction in the structure of the water layers close to the NP. This stage lasts around 1 ns. Secondly, at longer times, the temperature in the solution becomes almost uniform, but still lower than that of the NP. By this stage, the salt ions are heavily depleted from a proximal region about 15–25 Å from the NP surface, and have accumulated and clustered beyond this region. The segregation of ions and water molecules is greatest after about 2.2 ns, and then the ions start to diffuse back into the proximal zone.

These are interesting effects, but the microscopic explanation is not straightforward. The larger displacement of the ions compared to the water molecules could be seen as a thermophoretic (Soret) effect, but this mainly occurs after 1 ns when the temperature gradient in the solution has already passed its maximum. That is not to say that the system has reached equilibrium, because the NP is still at higher temperature than the solution, but the flow of heat through the solution is apparently very slow. The equilibrium self-diffusion coefficients under ambient conditions do not yield any clues: near saturation, the experimental values for water[73,74] and the ions[75,76] are similar; and in classical simulations, water has a higher value than the ions.[77] Therefore, this looks like a nonequilibrium and transient phenomenon in which the ions are transported rapidly through the water network in the proximal zone, and then cluster in the distal zone.

The observations in the present work are consistent with a NP-mediated mechanism for NPLIN. If ions are depleted from a proximal region around the NP surface, and clustered beyond that region, then perhaps subsequent cooling of the solution leads to nucleation in

the region where the clustering has been enhanced. This effect has not been captured in the simulations because it was not possible to simulate the surrounding bulk solution in a realistic manner. Essentially, the bulk solution should act as a heat sink, and a protocol for mimicking this will have to be designed very carefully. Even though the local and average ion concentrations in the distal zone are not very different from the overall concentration in the system, the extent of ion clustering is high, and it only takes one nucleation event to be promoted by accumulation and clustering of solute, for crystallization to be associated with NP heating.

There are other external perturbations commonly used to induce primary nucleation. Two examples are mechanical shock and ultrasound (sonocrystallization).[78,79] Mechanical shock was traditionally used in the sugar industry in the 19$^{\text{th}}$ century to promote nucleation.[80] Ultrasound has been employed in the pharmaceutical industry to reduce induction times and to produce smaller particles.[81] In both of these cases it is considered that formation of cavities and pressure waves are the causes of nucleation, but as yet there are only qualitative pictures of the mechanisms and the dynamics involved. For example, the spatial and temporal location of nucleation relative to cavity formation, and the localized supersaturations involved, are not known. These external stimuli of nucleation have mechanistic features in common with the NP-heating mechanism for NPLIN. Therefore, not only are the effects reported in this work inherently interesting, they have potential implications for nucleation by other perturbations, and are therefore worthy of further investigation.

ACKNOWLEDGMENTS

This research was supported by the Engineering and Physical Sciences Research Council through the provision of a studentship to J.O.S.

REFERENCES

[1]B. A. Garetz, J. E. Aber, N. L. Goddard, R. G. Young, and A. S. Myerson, Phys. Rev. Lett. **77**, 3475 (1996).

[2]B. A. Garetz, J. Matic, and A. S. Myerson, Phys. Rev. Lett. **89**, 175501 (2002).

[3]X. Sun, B. A. Garetz, and A. S. Myerson, Cryst. Growth Des. **6**, 684 (2006).

[4]J. Tyndall, Philos. Mag. **37**, 384 (1869).

[5]A. Tam, G. Moe, and W. Happer, Phys. Rev. Lett. **35**, 1630 (1975).

[6]T. Okutsu, K. Nakamura, H. Haneda, and H. Hiratsuka, Cryst. Growth Des. **4**, 113 (2004).

[7]H. Adachi, K. Takano, Y. Hosokawa, T. Inoue, Y. Mori, H. Matsumura, M. Yoshimura, Y. Tsunaka, M. Morikawa, and S. Kanaya, Jpn. J. Appl. Phys. **42**, L798 (2003).

[8]B. C. Knott, M. F. Doherty, and B. Peters, J. Chem. Phys. **134**, 154501 (2011).

[9]Y. Liu, M. R. Ward, and A. J. Alexander, Phys. Chem. Chem. Phys. **19**, 3464 (2017).

[10]Y. Liu, M. H. van den Berg, and A. J. Alexander, Phys. Chem. Chem. Phys. **19**, 19386 (2017).

[11]A. J. Alexander and P. J. Camp, Cryst. Growth. Des. **9**, 958 (2009).

[12]C. Duffus, P. J. Camp, and A. J. Alexander, J. Am. Chem. Soc. **131**, 11676 (2009).

[13]M. R. Ward, I. Ballingall, M. L. Costen, K. G. McKendrick, and A. J. Alexander, Chem. Phys. Lett. **481**, 25 (2009).

[14]M. R. Ward and A. J. Alexander, Cryst. Growth Des. **12**, 4554 (2012).

[15]K. Fang, S. Arnold, and B. A. Garetz, Cryst. Growth Des. (2014), article ASAP.

[16]M. R. Ward, A. Rae, and A. J. Alexander, Cryst. Growth Des. **15**, 4600 (2015).

[17]M. R. Ward, A. M. Mackenzie, and A. J. Alexander, Cryst. Growth Des. **16**, 6790 (2016).

[18]M. Nardone and V. G. Karpov, Phys. Chem. Chem. Phys. **14**, 13601 (2012).

[19]V. G. Karpov, M. Nardone, and N. I. Grigorchuk, Appl. Phys. Lett. **86**, 075463 (2012).

[20]M. R. Ward, W. J. Jamieson, C. A. Leckey, and A. J. Alexander, J. Chem. Phys. **142**, 144501 (2015).

[21]J. R. Adleman, D. A. Boyd, D. G. Goodwin, and D. Psaltis, Nano Lett. **9**, 4417 (2009).

[22]E. Lukianova-Hleb, Y. Hu, L. Latterini, L. Tarpani, S. Lee, R. A. Drezek, J. H. Hafner, and D. O. Lapotko, ACS Nano **4**, 2109 (2010).

[23]A. Siems, S. A. L. Weber, J. Boneberg, and A. Plech, New J. Phys. **13**, 043018 (2011).

[24]M. T. Carlson, A. J. Green, and H. H. Richardson, Nano Lett. **12**, 1534 (2012).

[25]Z. Qin and J. C. Bischof, Chem. Soc. Rev. **41**, 1191 (2012).

[26]Z. Fang, Y.-R. Zhen, O. Neumann, A. Polman, F. J. G. de Abajo, P. Nordlander, and N. J. Halas, Nano Lett. **13**, 1736 (2013).

[27]J. Lombard, T. Biben, and S. Merabia, Phys. Rev. Lett. **112**, 105701 (2014).

[28]K. Sasikumar and P. Keblinski, J. Chem. Phys. **141**, 234508 (2014).

[29]X. Chen, A. Munjiza, K. Zhang, and D. Wen, J. Phys. Chem. C **118**, 1285 (2014).

[30]Original data are available from http://dx.doi.org/[to be completed on acceptance].

[31]M. Trypuć, U. Kiełkowska, and M. Chałat, J. Chem. Eng. Data **47**, 765767 (2002).

[32]W. L. Jorgensen, J. Chandrasekhar, J. D. Madura, R. W. Impey, and M. L. Klein, J. Chem. Phys. **79**, 926 (1983).

[33]D. J. Price and C. L., III. Brooks, J. Chem. Phys. **121**, 10096 (2004).

[34]A. A. Chialvo and P. T. Cummings, Adv. Chem. Phys. **109**, 115 (1999).

[35]D. M. Sherman and M. D. Collings, Geochem. Trans. **3**, 102 (2002).

[36]D. Corradini, M. Rovere, and P. Gallo, J. Chem. Phys. **143**, 114502 (2015).

[37]L. X. Dang, J. Am. Chem. Soc. **117**, 6954 (1995).

[38]X. Sun, T. Chang, Y. Cao, S. Niwayama, W. L. Hase, and L. X. Dang, J. Phys. Chem. B **113**, 6473 (2009).

[39]I. S. Joung and T. E., III. Cheatham, J. Phys. Chem. B **113**, 13279 (2009).

[40]"LAMMPS Molecular Dynamics Simulator," (1995), http://lammps.sandia.gov.

[41]S. Plimpton, J. Comp. Phys. **117**, 1 (1995).

[42]W. L. Jorgensen, D. S. Maxwell, and J. Tirado-Rives, J. Am. Chem. Soc. **118**, 11225 (1996).

[43]L. X. Dang and D. Feller, J. Phys. Chem. B **104**, 4403 (2000).

[44]K. J. McEwan and P. A. Madden, J. Chem. Phys. **97**, 8748 (1992).

[45]D. Chakraborty and G. N. Patey, J. Phys. Chem. Lett. **4**, 573 (2013).

[46]D. Chakraborty and G. N. Patey, Chem. Phys. Lett. **587**, 25 (2013).

[47]P. R. ten Wolde and D. Frenkel, J. Chem. Phys. **109**, 9901 (1998).

[48]J. Wedekind and D. Reguera, J. Chem. Phys. **127**, 154516 (2007).

[49]P. J. Steinhardt, D. R. Nelson, and M. Ronchetti, Phys. Rev. B **28**, 784 (1983).

[50]P. R. ten Wolde, M. J. Ruiz-Montero, and D. Frenkel, Phys. Rev. Lett. **75**, 2714 (1995).

[51]P. R. ten Wolde, M. J. Ruiz-Montero, and D. Frenkel, J. Chem. Phys. **104**, 9932 (1996).

[52]J. R. Errington and P. G. Debenedetti, J. Chem. Phys. **118**, 2256 (2003).

[53]S. Auer and D. Frenkel, J. Chem. Phys. **120**, 3015 (2004).

[54]Y. Wang, S. Teitel, and C. Dellago, J. Chem. Phys. **122**, 214722 (2005).

[55]W. Lechner and C. Dellago, J. Chem. Phys. **129**, 114707 (2008).

[56]W. Lechner, C. Dellago, and P. G. Bolhuis, Phys. Rev. Lett. **106**, 085701 (2011).

[57]F. Bresme, A. Lervik, D. Bedeaux, and S. Kjelstrup, Phys. Rev. Lett. **101**, 020602 (2008).

[58]J. Muscatello, F. Römer, J. Sala, and F. Bresme, Phys. Chem. Chem. Phys. **13**, 19970 (2011).

[59]J. A. Armstrong and F. Bresme, J. Chem. Phys. **139**, 014504 (2013).

[60]J. Armstrong, A. Lervik, and F. Bresme, J. Phys. Chem. B **117**, 14817 (2013).

[61]J. Armstrong, C. D. Daub, and F. Bresme, J. Chem. Phys. **143**, 036101 (2015).

[62]P. Wirnsberger, D. Fijan, A. Šarić, M. Neumann, C. Dellago, and D. Frenkel, J. Chem. Phys. **144**, 224102 (2016).

[63]P. Wirnsberger, D. Fijan, R. A. Lightwood, A. Šarić, C. Dellago, and D. Frenkel, Proc. Natl. Acad. Sci. (USA) **114**, 4911 (2017).

[64]P. Jungwirth and D. J. Tobias, J. Phys. Chem. B **105**, 1046810472 (2001).

[65]P. Jungwirth and D. J. Tobias, J. Phys. Chem. B **106**, 63616373 (2002).

[66]S. Pal and F. Müller-Plathe, J. Phys. Chem. B **109**, 6405 (2005).

[67]D. M. Huang, C. Cottin-Bizonne, C. Ybert, and L. Bocquet, J. Phys. Chem. B **24**, 1442 (2008).

[68]If one assumes a simple linear molality profile $b(r) = b_{\rm bulk}(r-r_{\rm NP})/(r^*-r_{\rm NP})$ $(r_{\rm NP} \leq r \leq r^*)$ and $b(r) = b_{\rm bulk}$ $(r > r^*)$ where $r_{\rm NP} = 20$ Å is the NP radius, then with typical values of $r^* = 35$–45 Å, the criterion would be $\beta(r^*) \simeq 0.6$, which is close to that used here.

[69]C. T. Avedisian, J. Phys. Chem. Ref. Data **14**, 695 (1985).

[70]Y. Dou, L. V. Zhigilei, N. Winograd, and B. J. Garrison, J. Phys. Chem. A **105**, 2748 (2001).

[71]C. Vega and J. L. F. Abascal, Phys. Chem. Chem. Phys. **13**, 19663 (2011).

[72]S. Koneshan and J. C. Rasaiah, J. Chem. Phys. **113**, 8125 (2000).

[73]K. J. Müller and H. G. Hertz, J. Phys. Chem. **100**, 1256 (1996).

[74]J. S. Kim, Z. Wu, A. R. Morrow, A. Yethiraj, and A. Yethiraj, J. Phys. Chem. B **116**, 12007 (2012).

[75]R. H. Stokes, J. Am. Chem. Soc. **72**, 2243 (1950).

[76]V. Vitagliano and P. A. Lyons, J. Am. Chem. Soc. **78**, 1549 (1956).

[77]S. Chowdhuri and A. Chandra, J. Chem. Phys. **115**, 3732 (2001).

[78]S. W. Young, J. Am. Chem. Soc. **33**, 148 (1911).

[79]J. R. G. Sander, B. W. Zeiger, and K. S. Suslick, Ultrason. Sonochem. **21**, 1908 (2014).

[80]J. Bernstein, *Polymorphism in Molecular Crystals* (Oxford University Press, Oxford, 2007).

[81]G. Ruecroft, D. Hipkiss, T. Ly, N. Maxted, and P. W. Cains, Org. Process Res. Dev. **9**, 923 (2005).

TABLE I. Compositions of all systems. The concentration is given by the molality b, and the experimental molality at saturation is $b_{\mathrm{sat}} = 6.147$ mol kg^{-1} at $T = 293$ K.[31] $N(\mathrm{H_2O})$, $N(\mathrm{Na^+})$, $N(\mathrm{Cl^-})$, and $N(\mathrm{C})$ are, respectively, the numbers of water molecules, sodium ions, chloride ions, and carbon atoms, and N_{atom} is the total number of atoms.

b/mol kg^{-1}	b/b_{sat}	$N(\mathrm{H_2O})$	$N(\mathrm{Na^+}) = N(\mathrm{Cl^-})$	$N(\mathrm{C})$	N_{atom}	Nanoparticle
6.158	1.0	4507	500	0	14521	none
6.774	1.1	4097	500	0	13291	none
7.387	1.2	3757	500	0	12271	none
8.003	1.3	3468	500	0	11404	none
8.622	1.4	3219	500	0	10657	none
9.233	1.5	3006	500	0	10018	none
7.386	1.2	60122	8000	5851	202217	solid NP
7.386	1.2	60122	8000	3378	199744	hollow NP

TABLE II. Potential parameters for all atomic and ionic species used in the MD simulations. σ and ε are the LJ range and energy parameters, respectively, and q is the partial charge.

Species	q/e	σ/Å	ε/kcal mol^{-1}	Reference
O	−0.830	3.188	0.1020	33
H	+0.415	0.000	0.0000	33
Na^+	+1.000	2.350	0.1300	38
Cl^-	−1.000	4.400	0.1000	37
C	0.000	3.550	0.0635	42,43

FIG. 1. Panels (a) and (b) show, respectively, a solid nanoparticle, and a cutaway of a hollow nanoparticle. Panels (c) and (d) show simulation snapshots of crystalline ions satisfying the bond-order criterion at $b = 1.0b_{\mathrm{sat}}$ and $b = 1.5b_{\mathrm{sat}}$, respectively. Panels (e), (f), and (g) show, respectively, all ions, ions satisfying the distance-based criterion, and ions satisfying the bond-order criterion in a system with $b = 1.4b_{\mathrm{sat}}$.

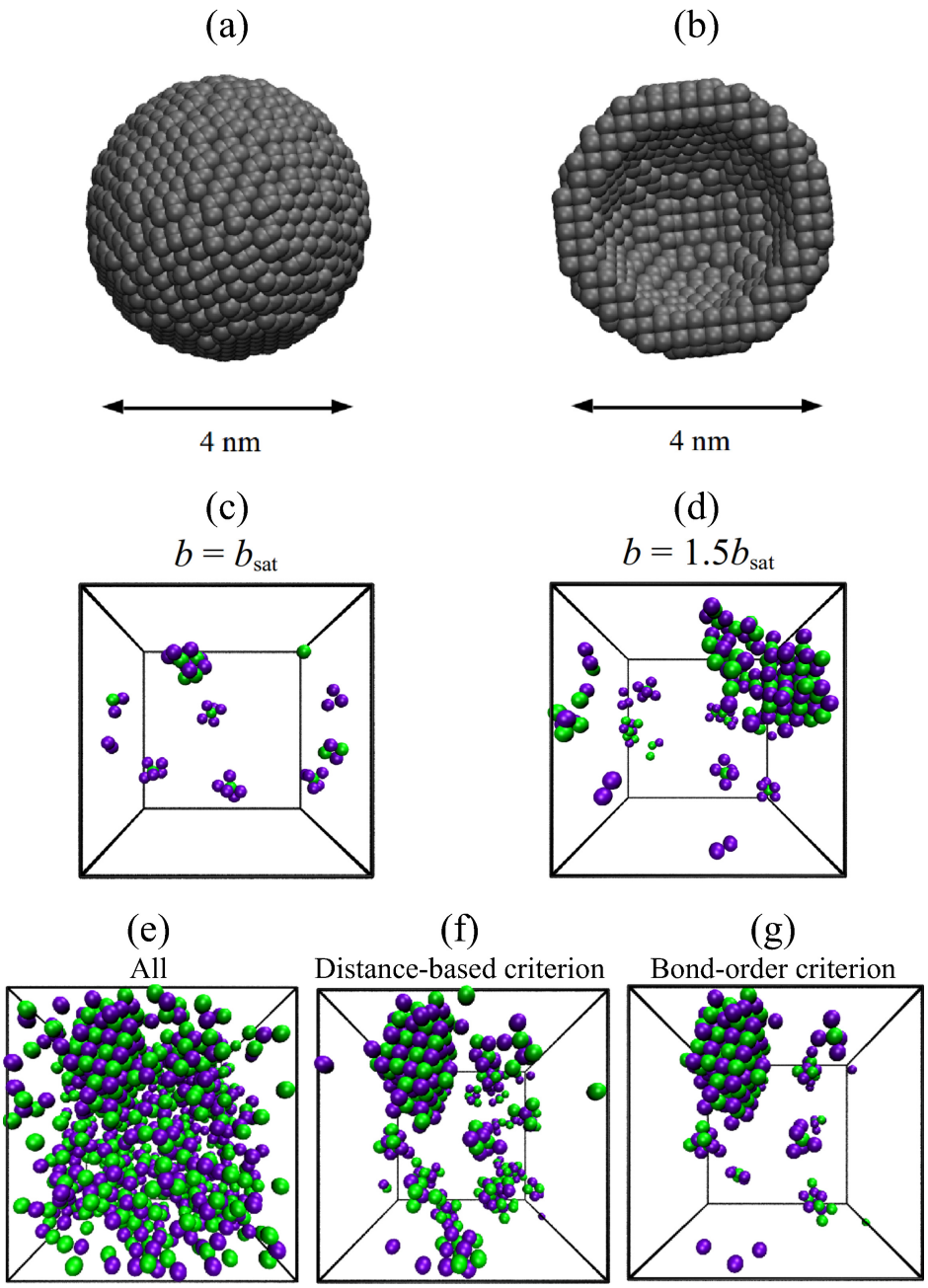

FIG. 2. Cluster properties from equilibrium simulations of NaCl(aq) at $T = 293$ K: (a) probability that an ion has N_n neighbors within a distance 3.80 Å, at concentrations $b = 1.0b_{sat}$ (black circles) and $b = 1.5b_{sat}$ (red squares); (b) crystalline-ion time correlation function at concentrations $1.0b_{sat}$–$1.5b_{sat}$; (c) fraction of ions in crystalline environments according to the simple distance-based criterion (black circles) and a local bond-order criterion (red squares); (d) residence time of ions in crystalline environments according to the simple distance-based criterion (black circles) and a local bond-order criterion (red squares).

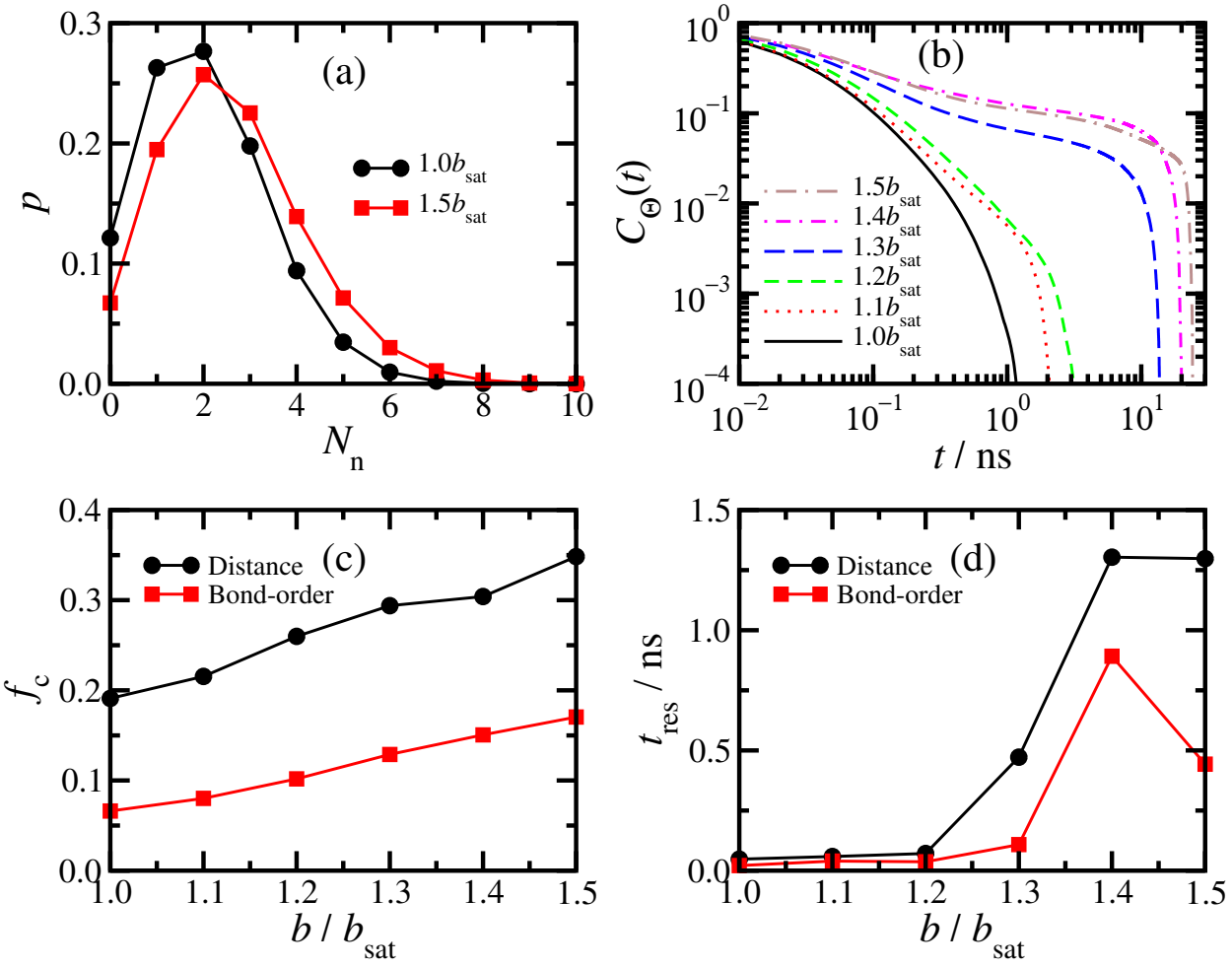

FIG. 3. Radial temperature profiles of (a) NP atoms, (b) water molecules, (c) sodium ions, and (d) chloride ions in simulations with a solid NP heated to $T_{\mathrm{NP}}(0) = 5293$ K. The vertical dashed lines indicate the position of the NP surface, and the solid arrows indicate the general trends with increasing time.

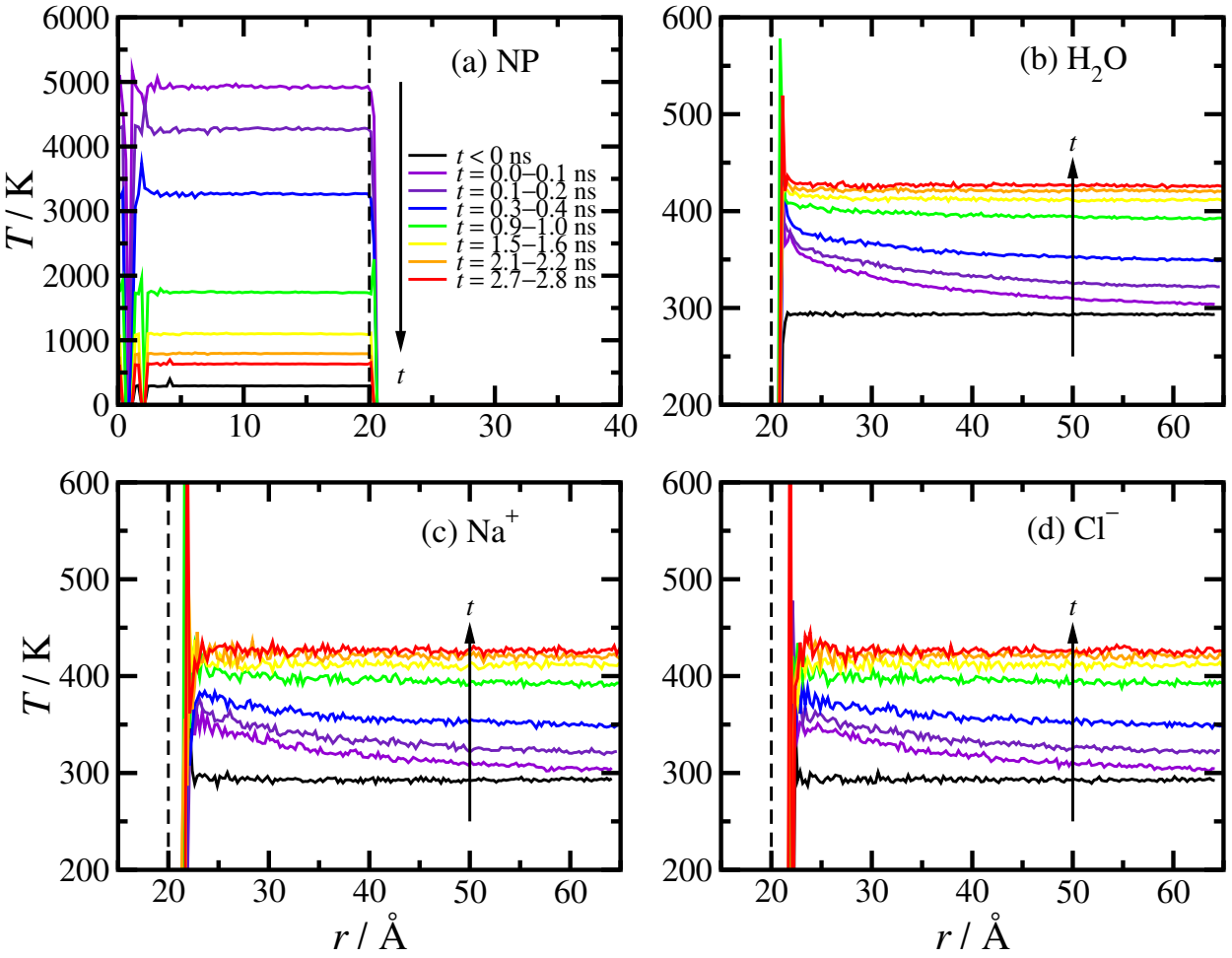

FIG. 4. Radial mass-density profiles of water molecules in simulations with a solid NP heated to [(a) and (b)] $T_{\mathrm{NP}}(0) = 5293$ K and [(c) and (d)] $T_{\mathrm{NP}}(0) = 10293$ K. Unscaled data are shown in (a) and (c) and scaled data using Eq. (3) are shown in (b) and (d). The vertical dashed lines indicate the position of the NP surface, and the solid arrows indicate the initial trend after heating.

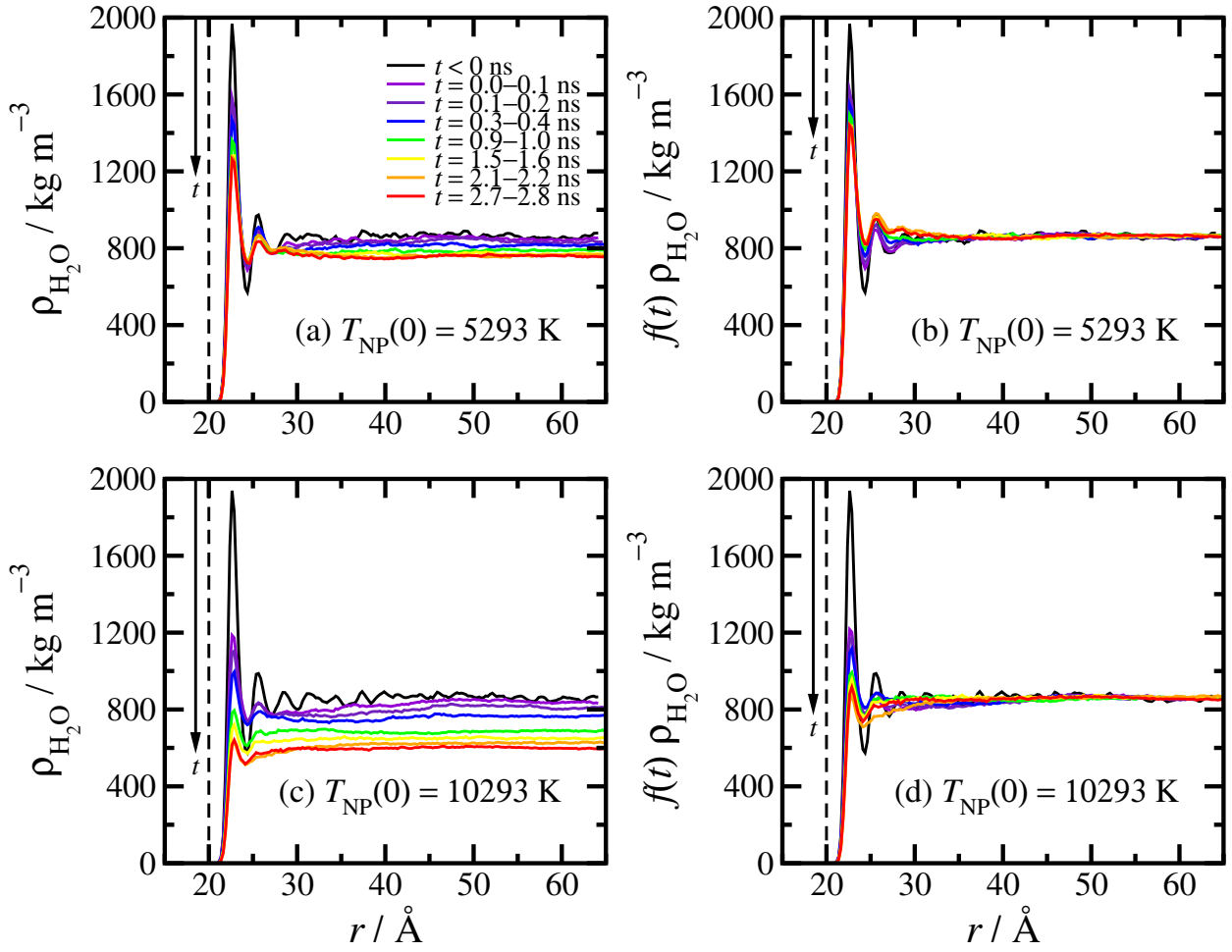

FIG. 5. (a) and (b) Orientational order parameters P_1 [Eq. (4)] and P_2 [Eq. (5)] of water molecules in simulations with a solid NP with $T_{\rm NP}(0) = 5293$ K (black circles), a solid NP with $T_{\rm NP}(0) = 10293$ K (red squares), and a hollow NP with $T_{\rm NP}(0) = 10293$ K (green diamonds). (c) The function $\beta(r)$ [Eq. (6)] from simulations with a solid NP with $T_{\rm NP}(0) = 5293$ K. The solid and dashed lines are for Na^+ and Cl^- ions, respectively, but the results are almost identical. The vertical dashed line indicates the position of the NP surface, and the solid arrow indicates the general trend after heating. (d) The radius where $\beta(r^*) = 2/3$. The colors/symbols are the same as in (a); data for Na^+ and Cl^- ions are shown as filled symbols/solid lines and open symbols/dashed lines, respectively, but the results are almost identical. (e) and (f) Fractions of ions in crystalline environments using the distance-based criterion (e) and the bond-order criterion (f). The colors/symbols are the same as in (a).

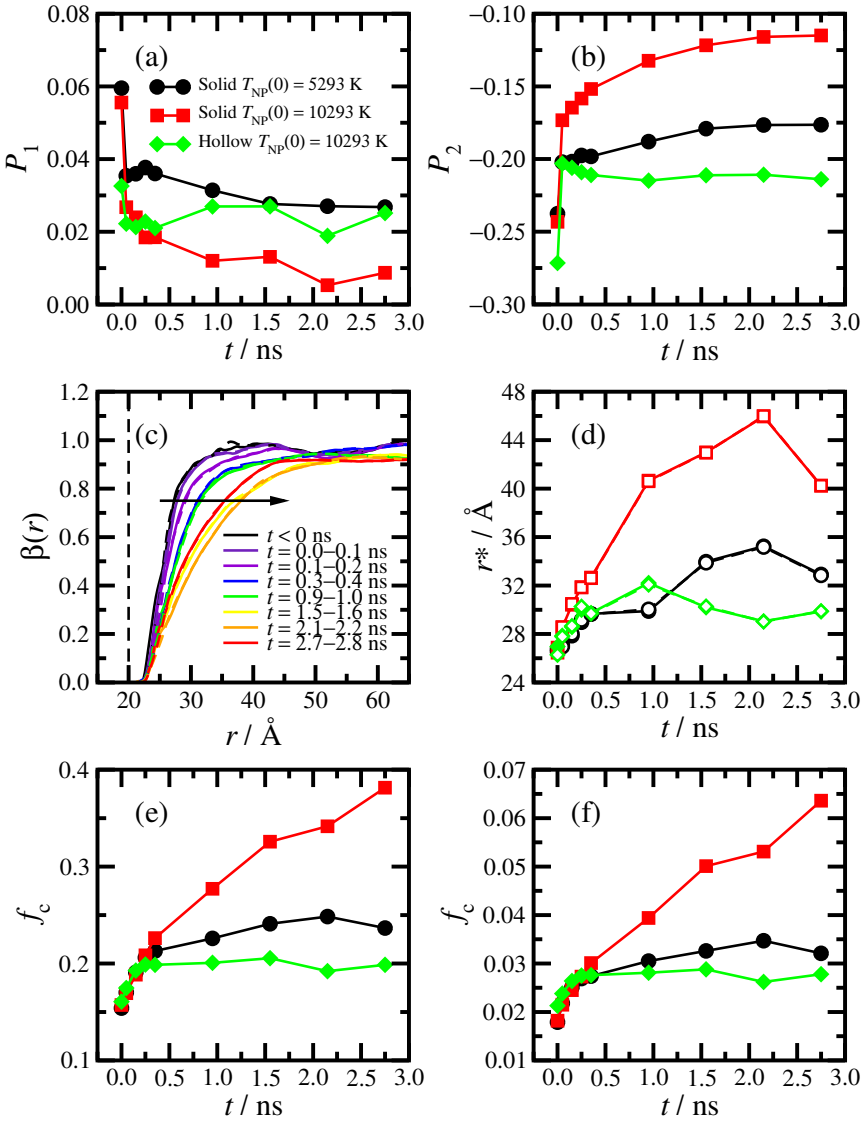

FIG. 6. Radial mass-density profiles of sodium ions [(a) and (b)] and chloride ions [(c) and (d)] in simulations with a solid NP heated to $T_{\mathrm{NP}}(0) = 5293$ K. (a) and (c) show unscaled data, and (b) and (d) show scaled data using Eq. (3). The vertical dashed lines indicate the position of the NP surface, and the solid arrows indicate the initial trend after heating.

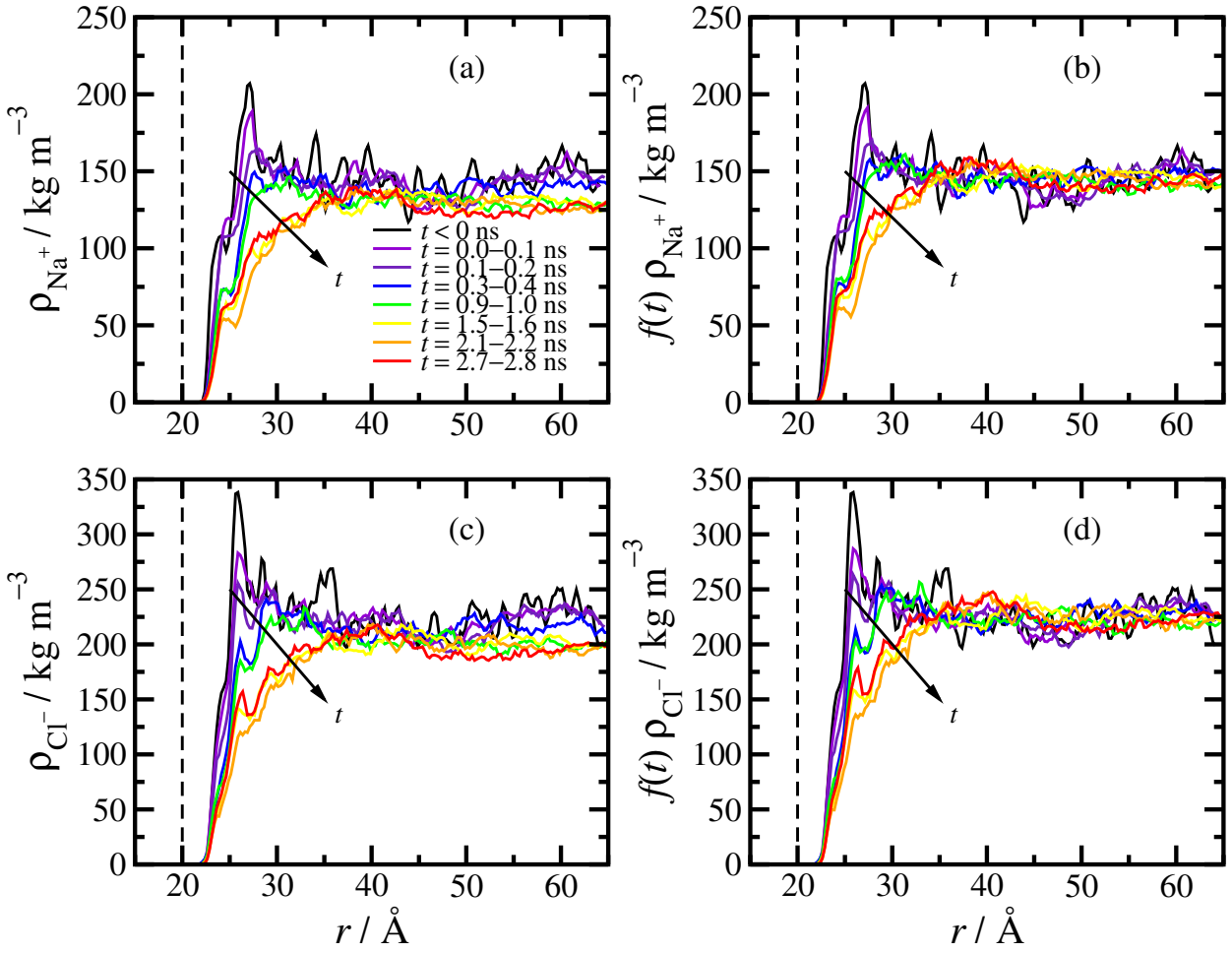

FIG. 7. Radial molality profiles of sodium ions [(a) and (c)] and chloride ions [(b) and (d)] in simulations with a solid NP heated to $T_{\mathrm{NP}}(0) = 5293$ K [(a) and (b] and $T_{\mathrm{NP}}(0) = 10293$ K [(c) and (d]. The vertical dashed lines indicate the position of the NP surface, and the solid arrows indicate the initial trend after heating.

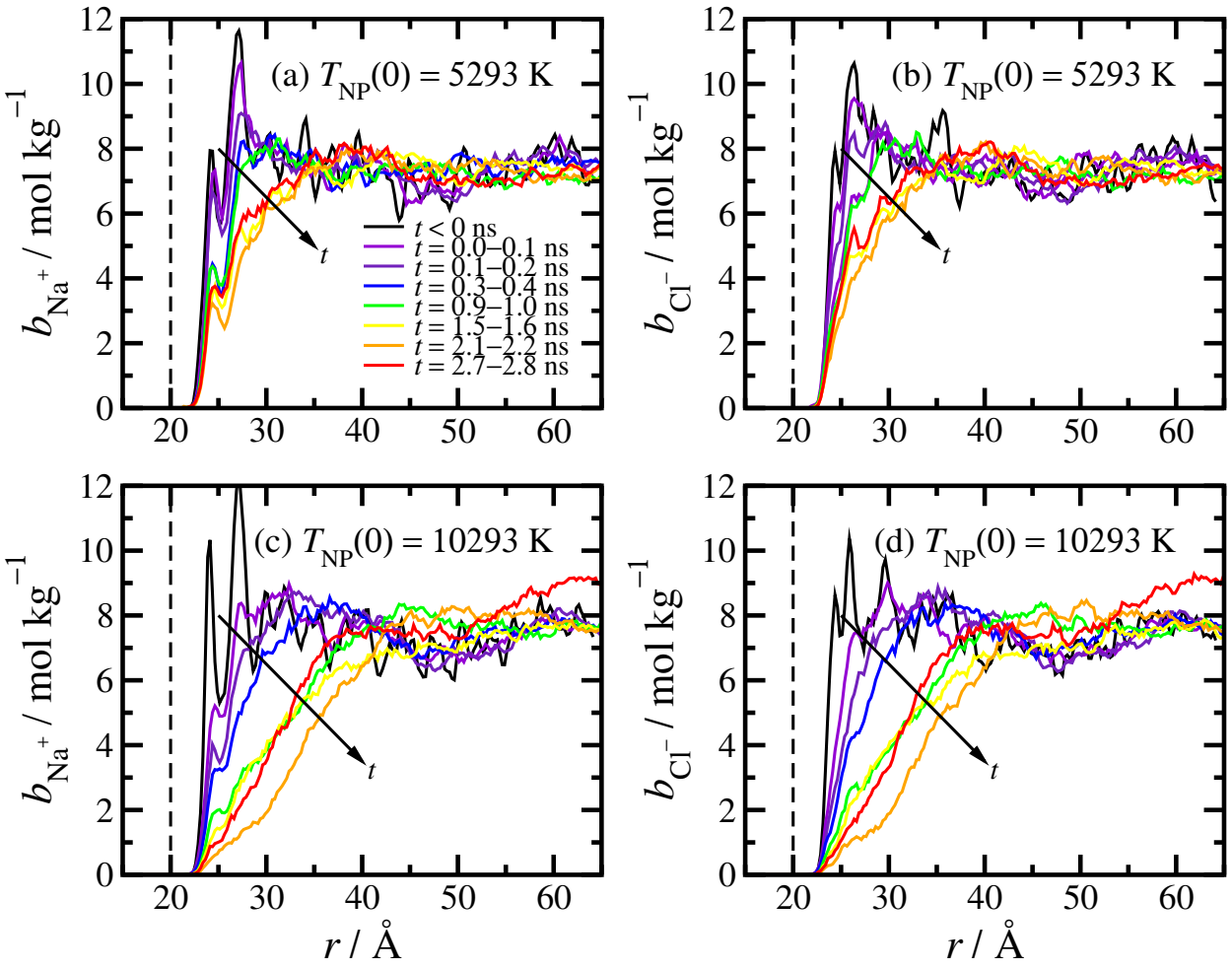

FIG. 8. Radial temperature profiles of (a) NP atoms, (b) water molecules, (c) sodium ions, and (d) chloride ions in simulations with a solid NP heated to $T_{\mathrm{NP}}(0) = 10293$ K. The vertical dashed lines indicate the position of the NP surface, and the solid arrows indicate the general trends with increasing time.

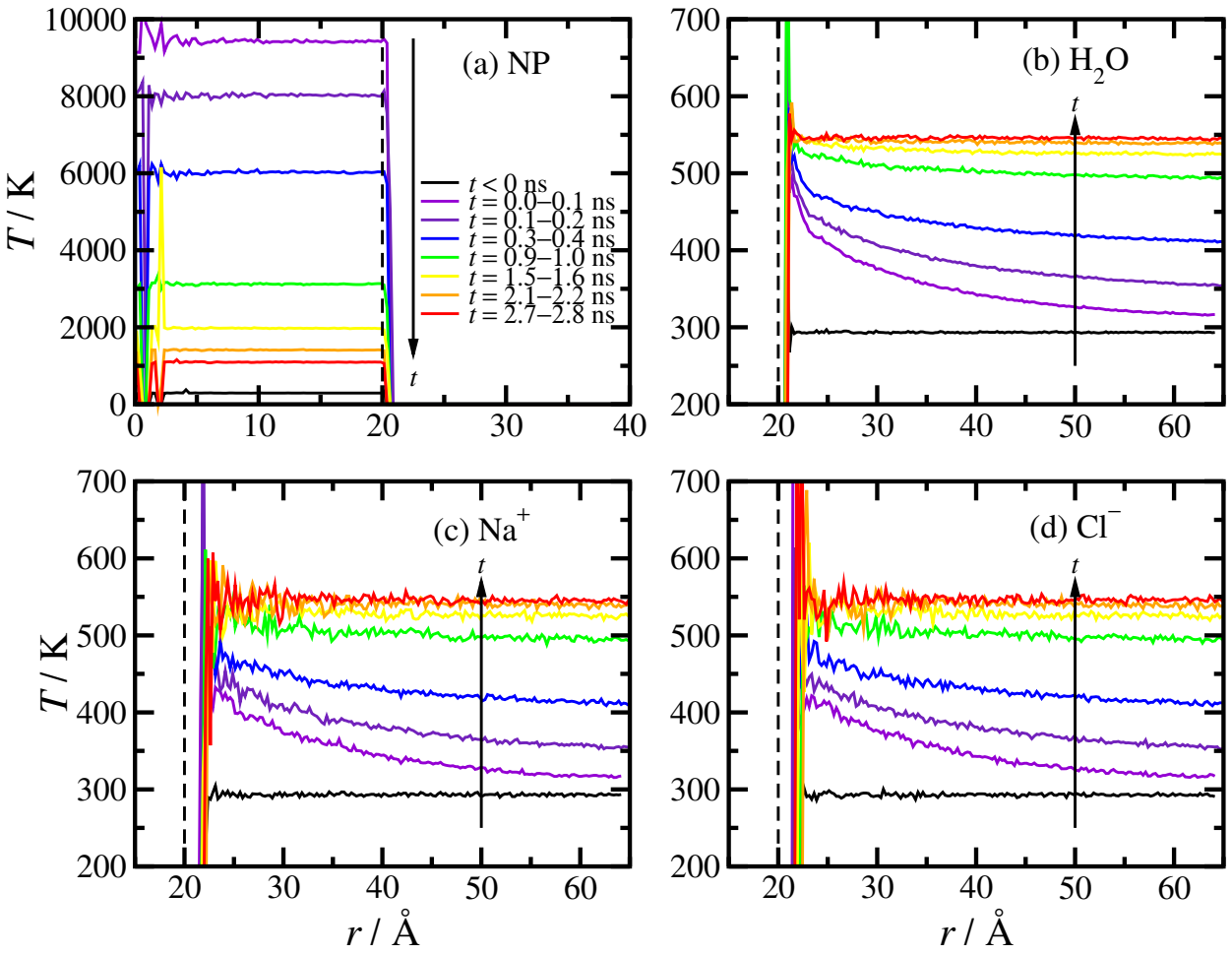

FIG. 9. Radial mass-density profiles of sodium ions [(a) and (b)] and chloride ions [(c) and (d)] in simulations with a solid NP heated to $T_{\mathrm{NP}}(0) = 10293$ K. (a) and (c) show unscaled data, and (b) and (d) show scaled data using Eq. (3). The vertical dashed lines indicate the position of the NP surface, and the solid arrows indicate the initial trend after heating.

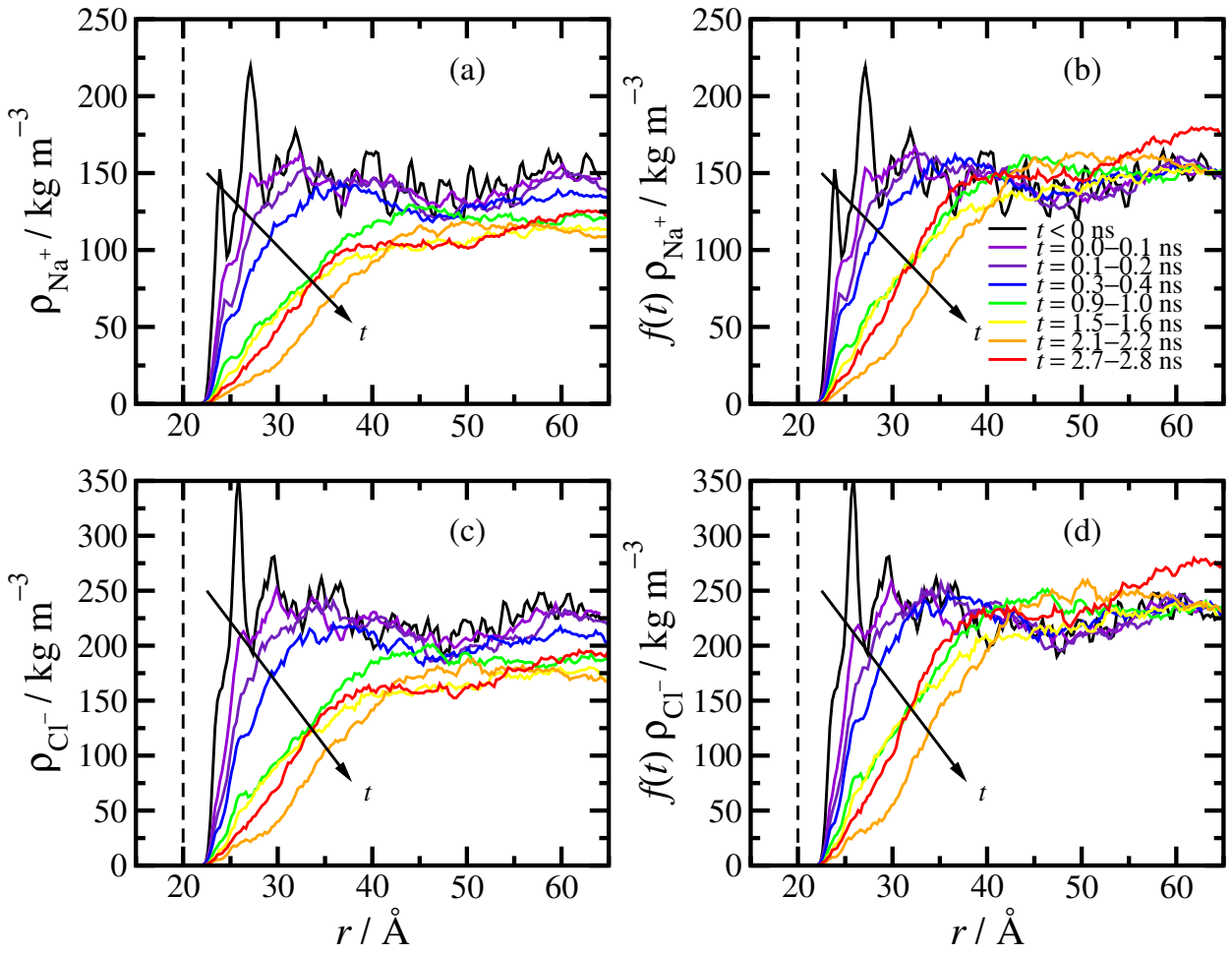

FIG. 10. (Multimedia view) Snapshots from simulations with a solid NP heated to $T_{\mathrm{NP}}(0) = 10293$ K. Images (a)–(d) show slices of thickness 4 Å through the center of the solid NP: (a) before heating; (b) 0.4 ns after heating; (c) 1.6 ns after heating; (d) 2.8 ns after heating. A movie is available online. Images (e) and (f) show ions satisfying the distance-based cluster criterion at equilibrium and 2.8 ns after heating, respectively. Images (g) and (h) show ions satisfying the bond-order cluster criterion at equilibrium and 2.8 ns after heating, respectively. Color scheme: C (gray); O (red); H (white); Na^+ (purple); Cl^- (green).

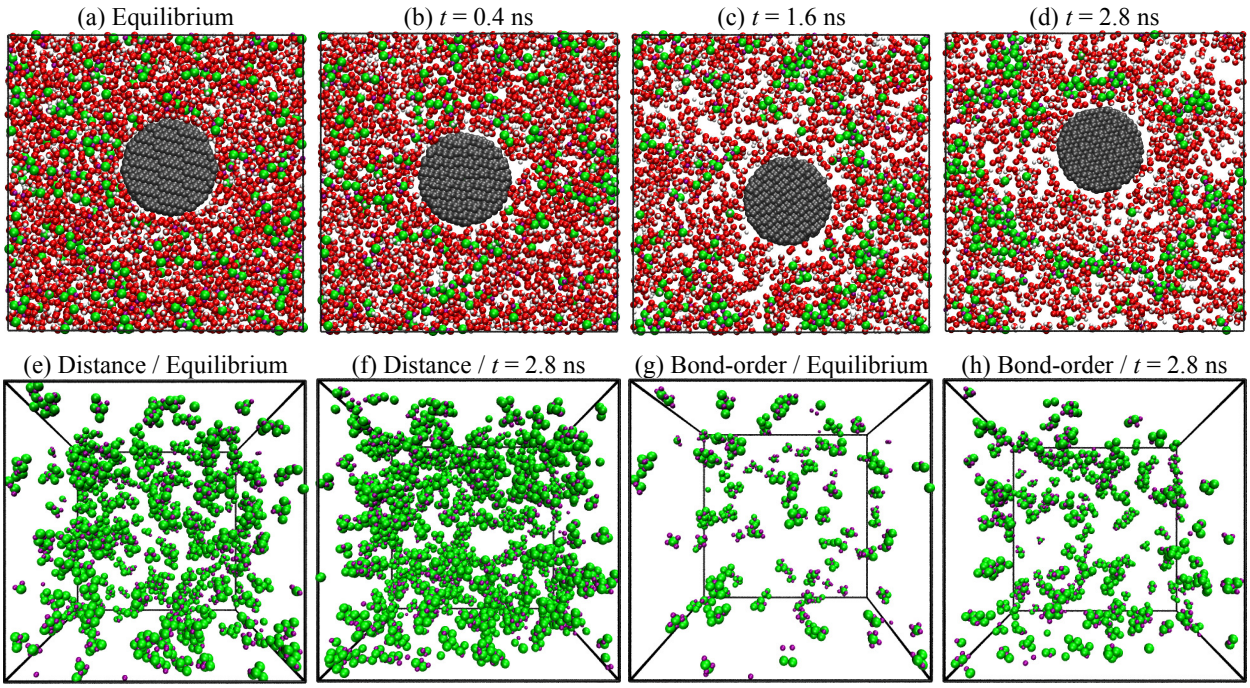

FIG. 11. Radial temperature profiles of (a) NP atoms, (b) water molecules, (c) sodium ions, and (d) chloride ions in simulations with a hollow NP heated to $T_{\mathrm{NP}}(0) = 10293$ K. The vertical dashed lines indicate the position of the NP surface, and the solid arrows indicate the general trends after heating.

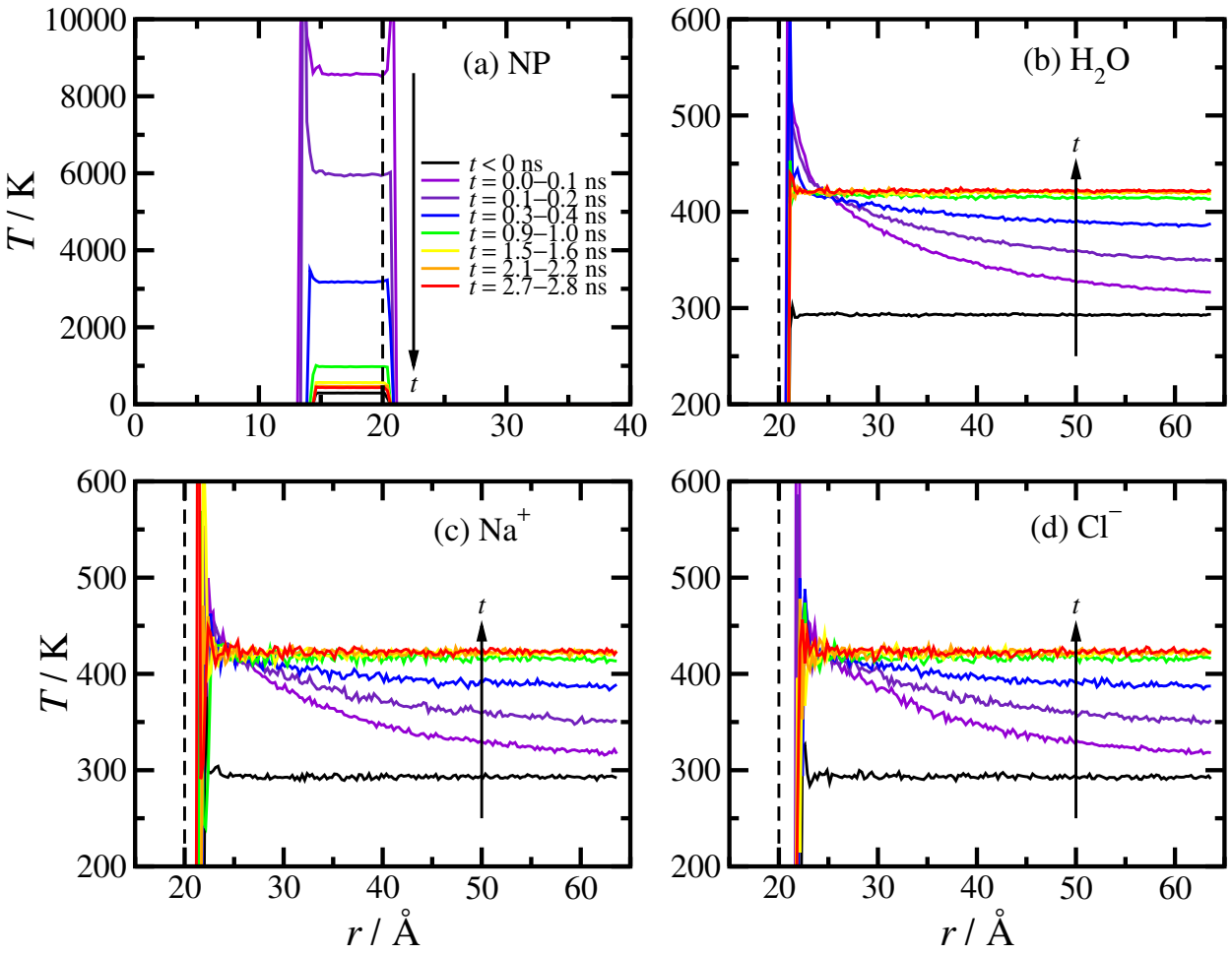

FIG. 12. Radial mass-density profiles of water [unscaled in (a), scaled by $f(t)$ in (b], and molality profiles of sodium ions (c) and chloride ions (d) in simulations with a hollow NP heated to $T_{\mathrm{NP}}(0) = 10293$ K. The vertical dashed lines indicate the position of the NP surface, and the solid arrows indicate the initial trend after heating.

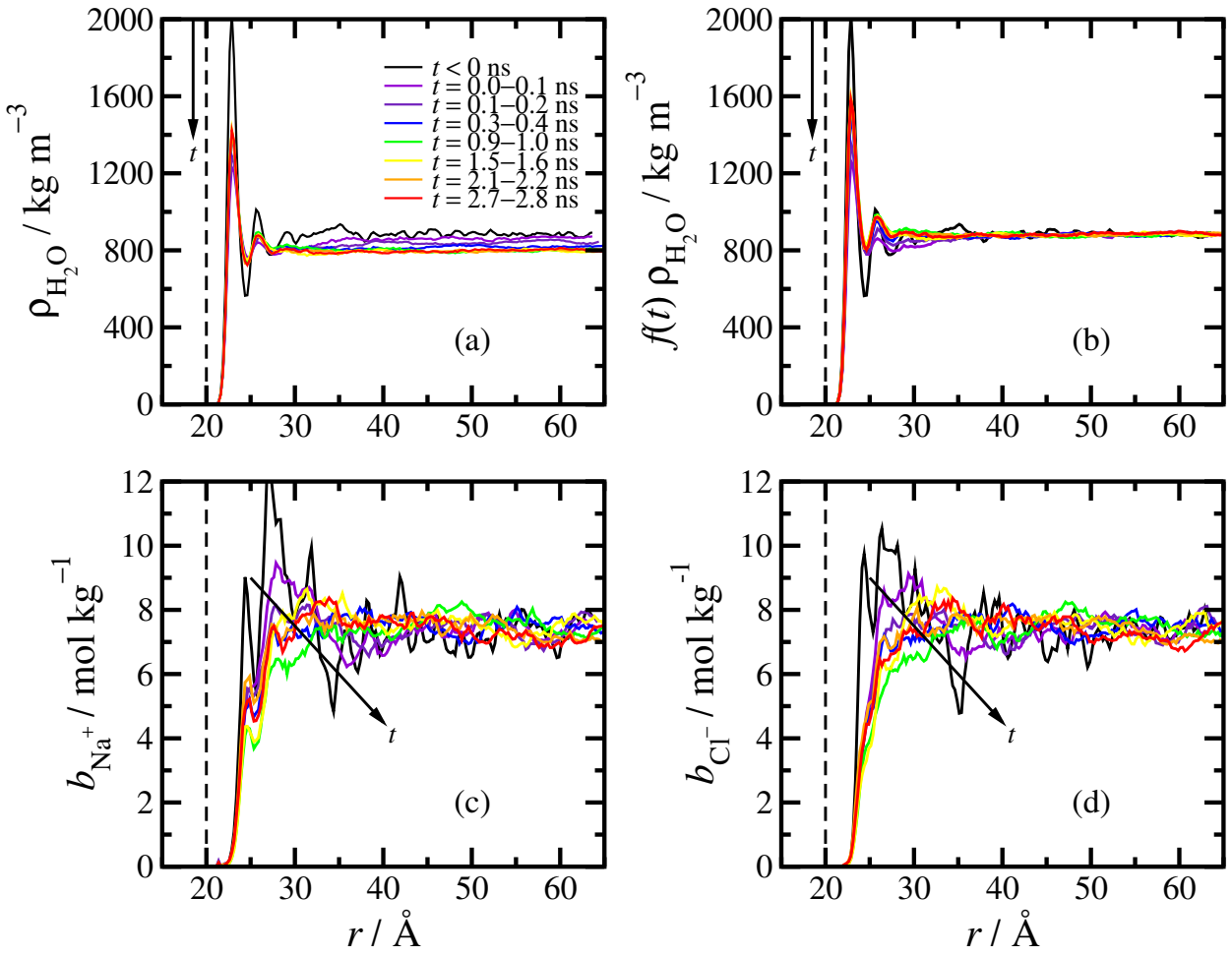

FIG. 13. Radial mass-density profiles of sodium ions [(a) and (b)] and chloride ions [(c) and (d)] in simulations with a hollow NP heated to $T_{\mathrm{NP}}(0) = 10293$ K. (a) and (c) show unscaled data, and (b) and (d) show scaled data using Eq. (3). The vertical dashed lines indicate the position of the NP surface, and the solid arrows indicate the initial trend after heating.